Market Clearing Model for Energy-constrained Virtual Power Plants with Uncertainty Based on Distributionally Robust Chance-constrained Optimization

Zhongkai Yi, *Member*, *IEEE*, Zihao Zhao, Ying Xu, *Senior Member*, *IEEE*, Yuhao Zhou, and Lun Yang, *Member*, *IEEE*

***Abstract*—With the increasing number of distributed flexible resources with energy storage capabilities in virtual power plants (VPPs), the traditional market clearing model that only includes quantity and price bids cannot fully unlock their potential flexibility. In light of this, we propose a market clearing model for energy-constrained virtual power plants (EC-VPPs) based on distributionally robust chance-constrained optimization (DRCCO) with moment information. Furthermore, to address the uncertainty of EC-VPPs in the electricity market, a pricing strategy for EC-VPPs is proposed. This strategy helps quantify the impact of uncertainty in EC-VPPs on the system economy. The proposed market clearing model is reformulated as a tractable mixed-integer second-order cone programming (MISOCP) problem via a two-sided distributionally robust chance-constrained convex reformulation method. Numerical simulations verify that the proposed pricing strategy offers fair incentives for both reserve providers and uncertain sources, and delivers an effective market mechanism for the EC-VPPs.**

***Index Terms*—Electricity market, market clearing, virtual power plant, pricing strategy, uncertainty, distributionally robust chance-constrained optimization.**

I. Introduction

With an increasing number of countries setting net-zero carbon emissions goals, the number of distributed flexible resources is rapidly increasing. Distributed flexible resources have great potential in improving the economy and security of power systems [1]. However, the low-capacity distributed flexible resources face major challenges in meeting the entry threshold to the electricity market. Virtual power plants (VPPs) constitute a new type of entity in the electricity market. They aggregate a group of distributed flexible resources to participate in electricity market operations, properly manage distributed flexible resources, and increase the flexibility of power systems [2].

China has been steadily advancing the development of VPPs supported by a series of policy measures [3]. Regarding peak shaving services, North China and Shanghai have explicitly allowed VPPs to operate as independent market entities, offering these services by acting as demand response (DR) resources. Regarding frequency regulation services, Jiangsu, China has included aggregated energy storage service providers as part of its frequency regulation resources, further expanding the application of VPPs.

Globally, the U.S., Australia, and Germany are actively exploring the participation of VPPs in their electricity markets. California, with its abundance of flexible resources, allows its independent system operator to handle peak shaving by developing plans through the day-ahead energy market [4]. In Australia, large-scale residential solar photovoltaic systems and energy storage facilities have been integrated into the grid to support its management [5]. Like California, Australia does not have a standalone peak shaving market but manages peak shaving through pre-clearing and real-time markets. As a pioneer of VPPs in Europe, Germany has integrated large amounts of wind, solar, and other renewable energy resources through its VPP platform [6]. Its peak shaving and frequency regulation are addressed primarily through frequency reserves and balancing markets, thereby setting a benchmark for VPP applications in Europe.

In an electricity market including VPPs, clearing is mostly centralized. A joint clearing model for the distribution-side market that considers the coupling relationship of multiple electricity market products has been proposed [7]. In this centralized model, a VPP aggregates its resources and submits them as a single market entity to the market operator responsible for market clearing. To ensure the coordinated optimization between the market and VPPs in a bilevel model, an upper-level model minimizes the overall operational cost

Manuscript received: July 15, 2024; revised: November 17, 2024; accepted: March 12, 2025. Date of CrossCheck: March 12, 2025. Date of online publication: April 17, 2025.

This work was supported by the National Natural Science Foundation of China (No. 52407089).

Z. Yi, Z. Zhao, and Y. Xu (corresponding author) are with the School of Electrical Engineering and Automation, Harbin Institute of Technology, Harbin, China (e-mail: yzk@hit.edu.cn; 23S006026@stu.hit.edu.cn; ying.xu@hit.edu.cn).

Y. Zhou is with State Grid Zhejiang Electric Power Co., Ltd., Ningbo, China (e-mail: 22S006077@stu.hit.edu.cn).

L. Yang is with the School of Automation Science and Engineering, Xi'an Jiaotong University, Xi'an, China (e-mail: yanglun@xjtu.edu.cn).

DOI: 10.35833/MPCE.2024.000744

of the active distribution network, whereas a lower-level model maximizes the advantages of each VPP agent [8]. The bilevel model emphasizes the interaction between the VPP decision-making and market response to these decisions. Another VPP model that considers the pricing strategy is proposed in [9]. Clearing is influenced by the pricing strategies adopted in the electricity market, further facilitating VPP participation in the market.

In the existing electricity market clearing approaches, VPPs often submit bids and operational constraints like those of conventional power generation units, including power and ramping constraints [10]. Order No. 841 issued by the U. S. Federal Energy Regulatory Commission requires electricity market designs to "account for the physical and operational characteristics of electric storage resources through bidding parameters or other means" [11]. However, owing to the presence of various types of general-purpose energy storage systems in VPPs, the existing constraints for VPPs cannot fully reflect their operational status. In fact, diverse energy constraints have been identified in VPP aggregation models [12]-[15]. However, they are often overlooked.

VPPs not only aggregate large amounts of energy storage, but also gather various types of wind and solar generation resources. Therefore, when VPPs receive dispatch instructions and response commands from the electricity market, inevitable deviations exist between the actual output of VPPs and dispatch instructions owing to uncertainties in the actual output of VPP components [16] - [20]. Considering the energy constraints and uncertainty of VPPs, traditional bidding models cannot adapt to the uncertainty and temporal coupling of power delivered by VPPs. Stochastic programming and robust optimization are common methods to address the uncertainty of market participants. For example, in [18] and [21], the scenario-based stochastic programming is used for a joint economic dispatch with renewable energy. In [22], the robust optimization is used to address the wind uncertainty in energy and reserve scheduling. However, the stochastic programming often requires knowledge of the true distribution of uncertainties, whereas the results of robust optimization tend to be overly conservative. Distributionally robust chance-constrained optimization (DRCCO) can address these problems in historical data while preventing overly conservative scheduling outcomes [23]-[26].

DRCCO has been applied to handle price uncertainties. For example, in [27] and [28], DRCCO is used to develop market clearing models that consider uncertainties in wind power and demand and infer uncertainties in locational marginal prices (LMPs). This is further expanded in [29] and [30] to explore the relationship between locational marginal uncertainty prices (LMUPs) and reserve LMPs. Although these models are applicable to power systems involving distributed resources while considering uncertainty, they are limited to traditional electricity market operation modes and require more consideration for the participation of energy-constrained VPPs (EC-VPPs). In [31], multiservice battery market clearing is introduced using DRCCO and considering multiservice pricing. However, the model only accounts for the simplest battery models and neglects grid congestion.

Various technical issues remain to be addressed. First, many VPPs possess energy-adjustable characteristics [11] - [14]. The formulation of a market clearing model for improving the energy adjustability of VPPs requires further investigation. Second, inevitable deviations occur between the VPP outputs and dispatch instructions issued by market operators [32]-[34]. Existing market clearing models neglect pricing related to these deviations. Third, although the rationality of the uncertain payment of renewable energy is demonstrated in [30], but the uncertainties of VPPs differ from those of renewable energy sources (e. g., batteries, energy storage systems, distributed generators, and DR loads). Research on the uncertainty in EC-VPPs remains insufficient. Therefore, an appropriate market clearing model should be devised to integrate the energy constraints and uncertainties of VPP while ensuring the power balance and economic operation of power systems.

To address the abovementioned issues, we propose a market clearing model for VPPs that considers energy constraints and uncertainty. The main contributions of this study are summarized as follows.

1) A universal pricing model is proposed considering energy constraints in VPPs, allowing EC-VPPs to simultaneously participate in the day-ahead energy and reserve markets.

2) The universal pricing model supports the collaborative pricing of active power and uncertainty in a VPP. We demonstrate the matching of uncertainty payments with reserve costs by using a rigid mathematical proof. The pricing model provides price incentives for managing uncertainty in VPPs.

3) We apply DRCCO with bilateral constraints to solve the VPP and uncertainty pricing problems. A moment-based method is used to transform the chance constraints. The original problem is transformed into a tractable mixed-integer second-order cone programming (MISOCP) problem without relying on specific information regarding the EC-VPP uncertainty.

The remainder of this paper is organized as follows. The concept of the EC-VPP with uncertainty is introduced in Section II. The chance-constrained market clearing model for EC-VPP is presented in Section III. Section IV presents the pricing strategy considering VPP uncertainty. Case studies are presented in Section V. Finally, we draw conclusions in Section VI.

II. Concept of EC-VPP with Uncertainty

A. Operation Mode of Electricity Market with VPP

The process of electricity market organization is illustrated in Fig. 1. The relationship among the market operator, VPP, and distributed energy resource owners is shown in Fig. 2.

The business operation model of electricity market with VPP can be divided into the following four stages.

1) The electricity market operator determines the relevant boundary conditions for unit and grid operations on the operational day. Once prepared, the operator releases information about day-ahead market transactions to market participants.

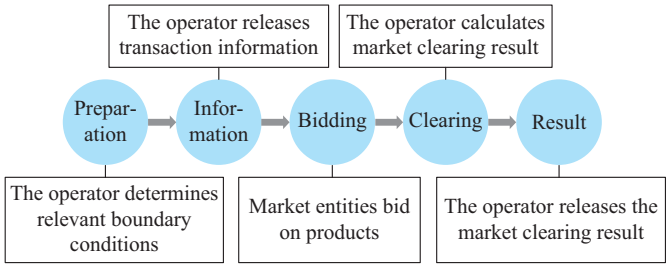

Fig. 1. Process of electricity market organization.

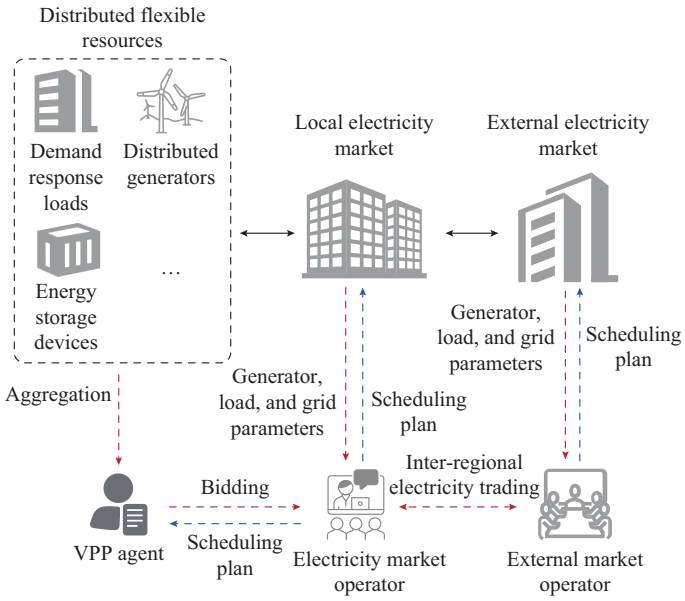

Fig. 2. Operation model of electricity market with VPP.

2) Electricity market participants submit products and their information. Based on the forecasting information from distributed flexible sources, the VPP aggregates the output ranges and operating costs of its internal resources to obtain the output pattern curve and aggregated cost characteristics of its flexible resources. The VPP agent submits the bid prices and output ranges for various market products to the electricity market operator. We consider that the VPP bids for the output limits, load limits, and prices of various products. In addition, to account for the energy state of VPP, its energy range and its initial and final energy states should be considered. Traditional power generation units also submit their output ranges and cost curves to the electricity market operators. Simultaneously, the grid control center determines the market product demand for each node of the grid in all periods and reports the demand curve to the trading center.

3) After collecting bids from all participants, the electricity market operator considers the output ranges and cost characteristics of various units and considers the prices of various market products in the electricity market. The operator performs unified market optimization clearing based on the product demand and system security operating constraints, determining the winning bid prices and quantities for each VPP as well as the equipment dispatch plan and product interaction plan between the external electricity market and local electricity market.

4) The electricity market operator publishes the day-ahead interaction plan, including the trading volumes and prices, to all market participants.

B. EC-VPP Model

VPPs aggregate various distributed flexible resources and participate in the electricity market through market operators that act as agents. Unlike conventional generators, VPPs are affected by their energy states because of the distributed flexible resources that provide grid services. To ensure that the grid dispatch demands on a VPP do not exceed its capacity to provide energy services, the VPP must submit the aggregated energy regulation range of its distributed flexible resources, that is, the boundary curve of its energy constraints.

We incorporate energy constraints and states into the VPP model. The VPP energy state range depends on the aggregation of its internal distributed flexible resources. Various methods for calculating the parameters of VPP aggregation models and energy state ranges have been proposed [10] - [13]. The VPP model considering the energy constraints, i.e., EC-VPP model, can be expressed as:

$$e_{i,t}=\theta_{i,t}e_{i,t-1}+\left(\eta^{\mathrm{b}}_{i,t}x^{\mathrm{b}}_{i,t}p^{\mathrm{VPP,b}}_{i,t}-\frac{x^{\mathrm{s}}_{i,t}}{\eta^{\mathrm{s}}_{i,t}}p^{\mathrm{VPP,s}}_{i,t}\right)\Delta t-\delta_{i,t} \tag{1}$$

$$\underline{e}_{i,t}\le e_{i,t}\le \bar{e}_{i,t} \tag{2}$$

$$\underline{e}_{i,\mathrm{fin}}\le e_{i,T}\le \bar{e}_{i,\mathrm{fin}} \tag{3}$$

$$0\le p^{\mathrm{VPP,s}}_{i,t}\le \bar{p}^{\mathrm{s}}_{i,t} \tag{4}$$

$$0\le p^{\mathrm{VPP,b}}_{i,t}\le \bar{p}^{\mathrm{b}}_{i,t} \tag{5}$$

$$p_{i,t}=x^{\mathrm{s}}_{i,t}p^{\mathrm{VPP,s}}_{i,t}-x^{\mathrm{b}}_{i,t}p^{\mathrm{VPP,b}}_{i,t} \tag{6}$$

$$x^{\mathrm{s}}_{i,t}+x^{\mathrm{b}}_{i,t}=1 \quad x^{\mathrm{s}}_{i,t},x^{\mathrm{b}}_{i,t}\in\{0,1\} \tag{7}$$

where t is the index of time slots; T is the scheduling horizon; i is the index of nodes in power systems; $e_{i,t}$ is the energy state of the i^{th} VPP at time t; $\theta_{i,t}$ is the energy dissipation rate of the i^{th} VPP at time t; $\eta^{\mathrm{s}}_{i,t}$ and $\eta^{\mathrm{b}}_{i,t}$ are the charging and discharging efficiency rates of the i^{th} VPP at time t, respectively; Δt is the time step; $p^{\mathrm{VPP,s}}_{i,t}$ and $p^{\mathrm{VPP,b}}_{i,t}$ are the sold and purchased power of the i^{th} VPP at time t, respectively; $\delta_{i,t}$ is the energy correction factor of the i^{th} VPP at time t; $\bar{e}_{i,t}$ and $\underline{e}_{i,t}$ are the upper and lower bounds for energy state of the i^{th} VPP at time t, respectively; $\bar{e}_{i,\mathrm{fin}}$ and $\underline{e}_{i,\mathrm{fin}}$ are the final upper and lower bounds for the energy state of the i^{th} VPP, respectively; $\bar{p}^{\mathrm{s}}_{i,t}$ and $\bar{p}^{\mathrm{b}}_{i,t}$ are the upper bounds for the sold and purchased power of the i^{th} VPP at time t, respectively; $x^{\mathrm{s}}_{i,t}$ and $x^{\mathrm{b}}_{i,t}$ are the introduced binary variables of the i^{th} VPP at time t; and $p_{i,t}$ is the power transmitted from the i^{th} VPP to electricity market at time t.

Distributed flexible resources primarily include devices with energy storage characteristics (e. g., batteries, energy storage systems, thermally controllable loads, and deferrable loads), distributed generators, and DR loads [35]. For energy storage devices, factors such as the charging and discharging rates and capacity may impose energy constraints. However, other flexible resources aggregated by VPPs also impact their operational status. The output of renewable energy gen-

eration equipment such as wind turbines and solar photovoltaic panels is strongly affected by weather conditions, which may lead to instability in the energy supply. The DR load balances supply and demand by adjusting the electricity consumption behavior. However, the user participation and response speed may become limiting factors.

To better understand EC-VPPs, the corresponding relationships between the parameters of EC-VPP model in (1)-(7) and several representative distributed flexible resources are listed in Table I.

TABLE I
RELATIONSHIPS BETWEEN PARAMETERS OF EC-VPP MODEL AND SEVERAL REPRESENTATIVE DISTRIBUTED FLEXIBLE RESOURCES

Parameters in EC-VPP model in (1)-(7)	Parameters of distributed flexible resources		
	Energy storage system	Distributed generator	DR load
e_t	SOC_t		$\sum_{t=1}^{T} d_t^{\mathrm{DR}}$
$\bar{p}_t^{\mathrm{b}}$	$\bar{p}_t^{\mathrm{c}}$	0	$\sum_{t=1}^{T} \bar{d}_t^{\mathrm{DR}} - d_t^{\mathrm{DR,B}}$
$\bar{p}_t^{\mathrm{s}}$	$\bar{p}_t^{\mathrm{d}}$	$\bar{p}_t^{\mathrm{DG}}$	$d_t^{\mathrm{DR,B}} - \sum_{t=1}^{T} \underline{d}_t^{\mathrm{DR}}$
$\underline{e}_t$	$\underline{SOC}_t$		$\sum_{t=1}^{T} \underline{d}_t^{\mathrm{DR}}$
$\bar{e}_t$	$\overline{SOC}_t$		$\sum_{t=1}^{T} \bar{d}_t^{\mathrm{DR}}$
θ_t	θ_t	1	1
$\eta_t^{\mathrm{b}}, \eta_t^{\mathrm{s}}$	$\eta_i^{\mathrm{c}}, \eta_i^{\mathrm{d}}$	1	1
δ_t	ΔSOC_t	Δp_t	Δw_t

In Table I, SOC_t is the state of charge (SOC) of energy storage system at time t; $\bar{p}_t^{\mathrm{c}}$ and $\bar{p}_t^{\mathrm{d}}$ are the charging and discharging power of energy storage system at time t, respectively; $\overline{SOC}_t$ and $\underline{SOC}_t$ are the upper and lower bounds for SOC_t at time t, respectively; ΔSOC_t is the charge variation caused by electric vehicles in the energy storage system at time t; $\bar{p}_t^{\mathrm{DG}}$ is the upper bound for the planned output of all distributed generators at time t; p_t^{DG} is the output of distributed generators at time t; Δp_t is the energy deviation at time t; d_t^{DR} is the planned DR load at time t; $d_t^{\mathrm{DR,B}}$ is the forecasting DR load at time t; $\bar{d}_t^{\mathrm{DR}}$ and $\underline{d}_t^{\mathrm{DR}}$ are the upper and lower bounds for the DR load at time t, respectively; Δw_t is the energy deviation caused by the DR load at time t; and η_i^{c} and η_i^{d} are the charging and discharging efficiency rates of energy storage system, respectively.

C. VPP Uncertainty

The inherent characteristics of distributed flexible resources inevitably lead to deviations between the actual output and dispatch instructions of a VPP. These uncertainties primarily originate from three sources: ① SOC forecasting error of energy storage system; ② forecasting error of renewable energy generation; and ③ DR deviation.

1) SOC Forecasting Error of Energy Storage System

The accuracy of SOC forecasts critically determines the VPP supply-demand balance capability. Inaccurate SOC forecasts force the VPP to procure additional reserves or incur penalty costs, thereby increasing the operational expenditure. Specifically, SOC forecasting errors amplify the reserve capacity costs.

2) Forecasting Error of Renewable Energy Generation

The variability in renewable energy generation, especially of solar and wind energy sources, introduces large uncertainties. Poor forecasting can lead to large deviations from dispatch instructions, often requiring the deployment of expensive fast-acting reserves to maintain grid stability. This type of error typically leads to the highest cost impact because it directly influences market clearing prices and reserve allocations.

3) DR Deviation

DR uncertainties impair the precision of load matching and peak shaving. Although DR deviations exhibit lower volatility than renewable sources, their cost implications become more pronounced when DR constitutes a core flexibility resource. A slow DR further increases reserve costs during real-time operations.

The combination of multiple uncertainties hinders the prediction of the overall VPP output and energy boundaries, leading to a decrease in the credibility of VPP model. The inevitable deviation caused by VPP uncertainty incurs additional costs for power systems [36]. The additional costs generated by the uncertainties must be paid by the load, which is an unfair situation. Additionally, price signals from market clearing do not accurately reflect the impact of uncertainty on system operations. Therefore, the cost of uncertainties must be analyzed. This can encourage entities with uncertain properties to improve their forecasting accuracy to reduce uncertainty.

III. CHANCE-CONSTRAINED MARKET CLEARING MODEL FOR EC-VPP

A. DRCCO-based Market Clearing Model

The market clearing model aims to minimize the total operational cost while satisfying various system operational constraints. Market participants can be divided into four categories: external electricity markets, local electricity markets, VPPs, and traditional power generators. The optimization objective function comprises operational costs of VPP and generators, power purchase costs from external electricity market, and reserve costs, expressed as:

$$\min C = \sum_{t=1}^{T}\sum_{i=1}^{I}[F_{i,t}^{\mathrm{VPP}} + F_{i,t}^{\mathrm{GEN}} + \Delta t(b_t^{\mathrm{PT}} p_t^{\mathrm{PT}} + b_{r,i,t}^{\mathrm{GEN}} r_{i,t})] \quad (8)$$

where $F_{i,t}^{\mathrm{VPP}}$ is the cost of the i^{th} VPP modeled by a piecewise linear function at time t; $F_{i,t}^{\mathrm{GEN}}$ is the cost of the i^{th} generator modeled by a quadratic function at time t; b_t^{PT} is the energy price of external electricity market at time t; p_t^{PT} is the active power of external electricity market at time t; $b_{r,i,t}^{\mathrm{GEN}}$ is the reserve price of the i^{th} node at time t; $r_{i,t}$ is the reserve power of the i^{th} generator at time t; and I is the scheduling node quantity.

Considering the power output range and reserve limitation, each generator should satisfy the following constraints:

$$\begin{cases} g_{i,t}+r_{i,t}\le \bar{g}_i \\ g_{i,t}-r_{i,t}\ge \underline{g}_i \end{cases} \tag{9}$$

where $g_{i,t}$ is the output of the i^{th} generator at time t; and $\bar{g}_i$ and $\underline{g}_i$ are the upper and lower bounds for the output of the i^{th} generator, respectively.

The system power balance is formulated as:

$$p_{i,t}^{\text{in}}=g_{i,t}+(p_{i,t}^{\text{VPP,s}}-p_{i,t}^{\text{VPP,b}})-d_{i,t}: \lambda_{i,t} \tag{10}$$

$$\sum p_{i,t}^{\text{in}}=0: \lambda_t^{\text{sys}} \tag{11}$$

$$-p_j^l\le \boldsymbol{\Psi}_j\, \boldsymbol{p}_t^{\text{in}}\le p_j^l \tag{12}$$

where $p_{i,t}^{\text{in}}$ is the power injection of the i^{th} node at time t; $d_{i,t}$ is the load of the i^{th} node at time t; $\boldsymbol{p}_t^{\text{in}}$ is a vector composed of the power at each node at time t; $\boldsymbol{\Psi}_j$ is the power transfer distribution factor matrix for line j; p_j^l is the power flow transmission limit of line j; and $\lambda_{i,t}$ and λ_t^{sys} are the dual variables of constraints (10) and (11), respectively.

The load at each node in the system is predicted, and the VPP output is planned. To balance the fluctuation of each uncertainty source, the output of generators and power injection must be adjusted to compensate for power deviation. The generators must balance the deviations allocated to their corresponding nodes by the system and ensure that sufficient reserves are available, as shown in (15)-(17). The power injection varies with the VPP output, load, and generator output, as expressed in (18). Moreover, the energy state of VPP is affected by random power deviations.

$$\tilde{p}_{i,t}=p_{i,t}+\xi_{i,t}^{\text{p}} \tag{13}$$

$$\tilde{d}_{i,t}=d_{i,t}-\xi_{i,t}^{\text{d}} \tag{14}$$

$$\tilde{g}_{i,t}=g_{i,t}-\alpha_{i,t}\boldsymbol{e}^{\text{T}}(\boldsymbol{\xi}_t^{\text{p}}+\boldsymbol{\xi}_t^{\text{d}}) \tag{15}$$

$$r_{i,t}\ge \left|\alpha_{i,t}\boldsymbol{e}^{\text{T}}(\boldsymbol{\xi}_t^{\text{p}}+\boldsymbol{\xi}_t^{\text{d}})\right| \tag{16}$$

$$\sum \alpha_{i,t}=1: \lambda_t^{\alpha} \tag{17}$$

$$\tilde{\boldsymbol{p}}_t^{\text{in}}=\boldsymbol{p}_t^{\text{in}}+(\boldsymbol{I}-\boldsymbol{\alpha}_t\boldsymbol{e}^{\text{T}})(\boldsymbol{\xi}_t^{\text{p}}+\boldsymbol{\xi}_t^{\text{d}}) \tag{18}$$

$$\tilde{e}_{i,t}=\theta_{i,t}e_{i,t-1}+\eta_{i,t}^{\text{b}}x_{i,t}^{\text{b}}(p_{i,t}^{\text{VPP,b}}+\xi_{i,t}^{\text{p}})\Delta t-\frac{1}{\eta_{i,t}^{\text{s}}}x_{i,t}^{\text{s}}(p_{i,t}^{\text{VPP,s}}+\xi_{i,t}^{\text{p}})\Delta t+\delta_{i,t} \tag{19}$$

where $\tilde{p}_{i,t}$ is the actual power of the i^{th} VPP at time t; $\tilde{d}_{i,t}$ is the actual load of the i^{th} node at time t; $\tilde{g}_{i,t}$ is the actual power of the i^{th} generator at time t; $\xi_{i,t}^{\text{p}}$ is the deviation power of the i^{th} VPP at time t; $\xi_{i,t}^{\text{d}}$ is the load deviation of the i^{th} node at time t; $\boldsymbol{e}$ is the vector of ones; $\boldsymbol{\xi}_t^{\text{p}}$ is the vector comprising the VPP power deviations; $\boldsymbol{\xi}_t^{\text{d}}$ is the vector comprising the load deviations; $\alpha_{i,t}$ is a balancing factor for system uncertainty of the i^{th} node at time t; $\tilde{\boldsymbol{p}}_t^{\text{in}}$ is the vector of actual power injection at time t; $\boldsymbol{\alpha}_t$ is a vector comprising factors $\alpha_{i,t}$; $\boldsymbol{I}$ is the identity matrix; $\tilde{e}_{i,t}$ is the actual energy state of the i^{th} VPP at time t; and λ_t^{α} is the dual variable of constraint (17).

Energy correction factor $\delta_{i,t}$ refers to additional changes in energy within a VPP caused by various factors. It reflects phenomena such as energy loss resulting from temperature differences under controlled loads [37]. Typically, this parameter is not considered in energy storage systems because it primarily focuses on the energy storage and release, whereas the energy correction factor involves dynamic changes related to usage and scheduling.

B. Uncertainty Reformulation Using Chance Constraint

We define chance constraints for $r_{i,t}$, p_j^l, and $\tilde{e}_{i,t}$. Assuming that the deviations $\boldsymbol{\xi}_i$ do not follow a specific distribution, we consider that its underlying distribution originates from an ambiguity set that shares the same mean and covariance matrix. The ambiguity set Ω_i for $\boldsymbol{\xi}_i$ is defined as:

$$\Omega_i:=\{\mathbb{P}|\mathbb{P}(\boldsymbol{\xi}_i)=1, E_{\mathbb{P}}(\boldsymbol{\xi}_i)=\mu, E_{\mathbb{P}}(\boldsymbol{\xi}_i\boldsymbol{\xi}_i^{\text{T}})=\boldsymbol{\Sigma}_i\} \tag{20}$$

where $\mathbb{P}$ is a probability distribution/function; $E_{\mathbb{P}}(\boldsymbol{\xi}_i)=\mu$ represents the mean of $\boldsymbol{\xi}_i$; and $E_{\mathbb{P}}(\boldsymbol{\xi}_i\boldsymbol{\xi}_i^{\text{T}})=\boldsymbol{\Sigma}_i$ represents the covariance matrix of $\boldsymbol{\xi}_i$.

The chance constraint for the reserve $r_{i,t}$ is shown in (21), and the chance constraint for p_j^l is given by (22).

$$\inf_{\mathbb{P}\in\Omega_t}\mathbb{P}(-r_{i,t}\le\alpha_{i,t}\boldsymbol{e}^{\text{T}}(\boldsymbol{\xi}_t^{\text{p}}+\boldsymbol{\xi}_t^{\text{d}})\le r_{i,t})\ge 1-\varepsilon \tag{21}$$

$$\inf_{\mathbb{P}\in\Omega_t}\mathbb{P}(-p_j^l\le\boldsymbol{\Psi}_j[\boldsymbol{p}_t^{\text{in}}+(\boldsymbol{I}-\boldsymbol{\alpha}_t\boldsymbol{e}^{\text{T}})(\boldsymbol{\xi}_t^{\text{p}}+\boldsymbol{\xi}_t^{\text{d}})]\le p_j^l)\ge 1-\varepsilon \tag{22}$$

where Ω_t is the ambiguity set of $\boldsymbol{\xi}_t^{\text{p}}+\boldsymbol{\xi}_t^{\text{d}}$; and ε is the risk tolerance level.

The uncertainty in VPP energy can be divided into two parts: energy state and energy boundary. The uncertainty constraint of VPP energy is expressed as:

$$\underline{e}_{i,t}+\xi_{i,t}^{\text{e}-}\le\tilde{e}_{i,t}\le\bar{e}_{i,t}+\xi_{i,t}^{\text{e}+} \tag{23}$$

where $\xi_{i,t}^{\text{e}-}$ and $\xi_{i,t}^{\text{e}+}$ are the prediction deviations of the lower and upper bounds for VPP energy constraint, respectively.

To address the energy boundary uncertainty, constraint (23) can be reformulated as:

$$\underline{e}_{i,t}+\xi_{i,t}^{\text{m}}-\xi_{i,t}^{\text{n}}\le\tilde{e}_{i,t}\le\bar{e}_{i,t}+\xi_{i,t}^{\text{m}}+\xi_{i,t}^{\text{n}} \tag{24}$$

$$\begin{cases} \xi_{i,t}^{\text{m}}=(\xi_{i,t}^{\text{e}+}+\xi_{i,t}^{\text{e}-})/2 \\ \xi_{i,t}^{\text{n}}=(\xi_{i,t}^{\text{e}+}-\xi_{i,t}^{\text{e}-})/2 \end{cases} \tag{25}$$

where $\xi_{i,t}^{\text{m}}$ and $\xi_{i,t}^{\text{n}}$ are the co-directional deviation and counter-directional deviation of the VPP energy boundaries, respectively.

In (24), $\xi_{i,t}^{\text{m}}$ is equivalent to the sum of the actual power deviations of the VPP, as expressed in (26). However, we assume that $\xi_{i,t}^{\text{n}}$ is symmetric.

$$\underline{e}_{i,t}-\xi_{i,t}^{\text{n}}\le\tilde{e}_{i,t}-\xi_{i,t}^{\text{m}}\le\bar{e}_{i,t}+\xi_{i,t}^{\text{n}} \tag{26}$$

Proposition 1 If $\xi_{i,t}^{\text{n}}$ is symmetric, the chance constraint for $\xi_{i,t}^{\text{n}}$ can be replaced by (27) to satisfy the convex reformulation condition.

$$\inf_{\mathbb{P}\in\Omega_t^{\text{n}}}\mathbb{P}(\underline{e}_{i,t}\le e_{i,t}+\xi_{i,t}^{\text{n}}\le\bar{e}_{i,t})\ge 1-\varepsilon \tag{27}$$

where Ω_t^{n} is the ambiguity set of $\xi_{i,t}^{\text{n}}$.

The proof is provided in Supplementary Material A. Transferring the uncertainty generated by predicting the VPP energy boundaries to its energy model, a comprehensive chance constraint for the VPP energy state is given by (28).

$$\inf_{\mathbb{P}\in\Omega_t^{\text{nm}}}\mathbb{P}(\underline{e}_{i,t}\le\tilde{e}_{i,t}+(\xi_{i,t}^{\text{n}}-\xi_{i,t}^{\text{m}})\le\bar{e}_{i,t})\ge 1-\varepsilon \tag{28}$$

where Ω_t^{nm} is the ambiguity set of $\xi_{i,t}^{\text{n}}-\xi_{i,t}^{\text{m}}$.

Due to the risk of infeasibility in modeling chance con-

straints individually, a joint chance constraint method can be adopted. It enforces individual chance constraints with an explicit analytical parametrization of risk tolerance through individual violation probabilities. This method admits the Bonferroni approximation of the joint chance constraint when the sum of individual violation probabilities is less than the overall violation probability, that is, $\sum \varepsilon_i \le \varepsilon$. A joint feasibility guarantee is provided even when the choice of individual violation probabilities is suboptimal [38]. Under these conditions, the violation probability of a single constraint can be considered as the total constraint probability divided by the total number of individuals.

$$\inf_{\mathbb{P}\in\Omega_t} \mathbb{P}(-r_{i,t} \le \alpha_i \boldsymbol{e}^{\mathrm{T}}(\boldsymbol{\xi}_t^{\mathrm{p}} + \boldsymbol{\xi}_t^{\mathrm{d}}) \le r_{i,t}, \forall i \in \Upsilon) \ge 1-\varepsilon_{all} \tag{29}$$

where Υ is the set of generators; and ε_{all} is the overall risk tolerance.

C. Two-sided Chance-constrained Convex Reformulation

Chance constraints such as (21), (22), and (28) are intractable. Inspired by [20], a chance constraint in the form of (30) can be reformulated as a set of deterministic inequalities given by (31).

$$\inf_{\mathbb{P}\in\Omega} \mathbb{P}(\left| \boldsymbol{a}^{\mathrm{T}}\boldsymbol{\xi} + b \right| \le U) \ge 1-\varepsilon \tag{30}$$

$$\begin{cases} y^2 + \boldsymbol{a}^{\mathrm{T}}\boldsymbol{\Sigma}\boldsymbol{a} \le \varepsilon(U-z)^2 \\ |b| \le y+z \\ 0 \le y \\ 0 \le z \le U \end{cases} \tag{31}$$

where y and z are the auxiliary variables; $\boldsymbol{\Sigma}$ is the covariance matrix of random vector $\boldsymbol{\xi}$; Ω is the ambiguity set defined with respect to $\boldsymbol{\xi}$; $\boldsymbol{a}$ and b denote the affine mappings; and U is the boundary.

The chance constraints in (21), (22), and (28) can be substituted as:

$$(y_{i,t}^{\mathrm{g}})^2 + (\alpha_{i,t}\boldsymbol{e}^{\mathrm{T}})\boldsymbol{\Sigma}_t(\alpha_{i,t}\boldsymbol{e}) \le \varepsilon(r_{i,t} - z_{i,t}^{\mathrm{g}})^2 : \mu_{i,t}^{\mathrm{g}} \tag{32}$$

$$0 \le y_{i,t}^{\mathrm{g}} + z_{i,t}^{\mathrm{g}} : \mu_{i,t}^{\mathrm{gt}} \tag{33}$$

$$0 \le y_{i,t}^{\mathrm{g}} : \mu_{i,t}^{\mathrm{gy}} \tag{34}$$

$$0 \le z_{i,t}^{\mathrm{g}} \le r_{i,t} : \mu_{i,t}^{\mathrm{gz-}}, \mu_{i,t}^{\mathrm{gz+}} \tag{35}$$

$$(y_{j,t}^{\mathrm{b}})^2 + [\boldsymbol{\Psi}_j(\boldsymbol{I} - \boldsymbol{\alpha}\boldsymbol{e}^{\mathrm{T}})]\boldsymbol{\Sigma}_t[\boldsymbol{\Psi}_j(\boldsymbol{I} - \boldsymbol{\alpha}\boldsymbol{e}^{\mathrm{T}})]^{\mathrm{T}} \le \varepsilon(p_j^l - z_{j,t}^{\mathrm{b}})^2 : \mu_{j,t}^{\mathrm{b}} \tag{36}$$

$$\left| \boldsymbol{\Psi}_j \boldsymbol{p}_t^{\mathrm{in}} \right| \le y_{j,t}^{\mathrm{b}} + z_{j,t}^{\mathrm{b}} : \mu_{j,t}^{\mathrm{b-}}, \mu_{j,t}^{\mathrm{b+}} \tag{37}$$

$$0 \le y_{j,t}^{\mathrm{b}} : \mu_{j,t}^{\mathrm{by}} \tag{38}$$

$$0 \le z_{j,t}^{\mathrm{b}} \le p_j^l : \mu_{j,t}^{\mathrm{bz-}}, \mu_{j,t}^{\mathrm{bz+}} \tag{39}$$

$$\sum_{\tau=1}^{t}\left[\left(\prod_{\upsilon=\tau}^{t-1}\theta_{i,\upsilon}\right)^2\left(x_{i,t}^{\mathrm{b}}\eta_i^{\mathrm{b}} - \frac{x_{i,\tau}^{\mathrm{s}}}{\eta_i^{\mathrm{s}}}\right)^2(\sigma_{i,\tau}^{\mathrm{p}})^2 + (\sigma_{i,t}^{\mathrm{e}})^2\right] + (y_{i,t}^{\mathrm{e}})^2 \le \varepsilon\left(\frac{\bar{e}_{i,t} - \underline{e}_{i,t}}{2} - z_{i,t}^{\mathrm{e}}\right)^2 : \mu_{i,t}^{\mathrm{e}} \tag{40}$$

$$\sum_{\tau=1}^{t}\left[\left(\prod_{\upsilon=\tau}^{t-1}\theta_{i,\upsilon}\right)\left(x_{i,t}^{\mathrm{b}}\eta_i^{\mathrm{b}}p_{i,\tau}^{\mathrm{VPP,b}} - \frac{x_{i,\tau}^{\mathrm{s}}}{\eta_i^{\mathrm{s}}}p_{i,\tau}^{\mathrm{VPP,s}} + \delta_{i,\tau}\right)\right] + \left(\prod_{\tau=1}^{t}\theta_{i,\tau}\right)e_{i,0} - \frac{\bar{e}_{i,t} + \underline{e}_{i,t}}{2} \le y_{i,t}^{\mathrm{e}} + z_{i,t}^{\mathrm{e}} : \mu_{i,t}^{\mathrm{e-}}, \mu_{i,t}^{\mathrm{e+}} \tag{41}$$

$$0 \le y_{i,t}^{\mathrm{e}} : \mu_{i,t}^{\mathrm{ey}} \tag{42}$$

$$0 \le z_{i,t}^{\mathrm{e}} \le \frac{\bar{e}_{i,t} - \underline{e}_{i,t}}{2} : \mu_{i,t}^{\mathrm{e-}}, \mu_{i,t}^{\mathrm{e+}} \tag{43}$$

where $\mu_{i,t}^{\mathrm{g}}$, $\mu_{i,t}^{\mathrm{gt}}$, $\mu_{i,t}^{\mathrm{gy}}$, $\mu_{i,t}^{\mathrm{gz-}}$, $\mu_{i,t}^{\mathrm{gz+}}$, $\mu_{j,t}^{\mathrm{b}}$, $\mu_{j,t}^{\mathrm{b-}}$, $\mu_{j,t}^{\mathrm{b+}}$, $\mu_{j,t}^{\mathrm{by}}$, $\mu_{j,t}^{\mathrm{bz-}}$, $\mu_{j,t}^{\mathrm{bz+}}$, $\mu_{i,t}^{\mathrm{e}}$, $\mu_{i,t}^{\mathrm{e-}}$, $\mu_{i,t}^{\mathrm{e+}}$, and $\mu_{i,t}^{\mathrm{ey}}$ are the dual variables; $\sigma_{i,t}^{\mathrm{p}}$ is the standard deviation of the variable $\boldsymbol{\xi}_t^{\mathrm{p}}$; $\boldsymbol{\Sigma}_t$ is the covariance matrix of the random vector $\boldsymbol{\xi}_t^{\mathrm{p}} + \boldsymbol{\xi}_t^{\mathrm{d}}$; $y_{i,t}^{\mathrm{g}}$, $z_{i,t}^{\mathrm{g}}$, $y_{i,t}^{\mathrm{b}}$, $z_{i,t}^{\mathrm{b}}$, $y_{i,t}^{\mathrm{e}}$, and $z_{i,t}^{\mathrm{e}}$ are the auxiliary variables; and $\sigma_{i,t}^{\mathrm{e}}$ is the standard deviation of the variable $\xi_{i,t}^{\mathrm{n}} - \xi_{i,t}^{\mathrm{m}}$.

Overall, using the transformation of bilateral chance constraints, the chance-constrained problem can be reformulated as an MISOCP problem in the following compact form:

$$\begin{cases} \min C \\ \text{s.t. (1), (3)-(7), (9)-(12), (17), (32)-(43)} \end{cases} \tag{44}$$

IV. Pricing Strategy Considering VPP Uncertainty

The Lagrangian function for the proposed MISOCP problem is presented in Supplementary Material A. Constraints (32)-(35) transformed from the chance constraint (21) are equivalent to:

$$r_{i,t} \ge \alpha_{i,t}\sqrt{\frac{\boldsymbol{e}^{\mathrm{T}}\boldsymbol{\Sigma}_t\boldsymbol{e}}{\varepsilon}} : \mu_{i,t}^{\mathrm{g,eq}} \tag{45}$$

where $\mu_{i,t}^{\mathrm{g,eq}}$ is the dual variable of constraint (45).

Because $y_{i,t}^{\mathrm{g}} \ge 0$, $z_{i,t}^{\mathrm{g}} \ge 0$, and $r_{i,t} \ge z_{i,t}^{\mathrm{g}} \ge 0$, constraint (32) can be transformed into (46). When $y_{i,t}^{\mathrm{g}} = z_{i,t}^{\mathrm{g}} = 0$, the decision variable $r_{i,t}$ can achieve the minimum value in (47). Constraints (32)-(35) can be simplified to (45) with equivalent constraints, because $y_{i,t}^{\mathrm{g}}$ and $z_{i,t}^{\mathrm{g}}$ are auxiliary variables. Under these conditions, (45) can be interpreted as a constraint on the reserve requirement. The reserve requirement is given by (48).

$$r_{i,t} \ge \frac{1}{\sqrt{\varepsilon}}\sqrt{(y_{i,t}^{\mathrm{g}})^2 + (\alpha_{i,t}\boldsymbol{e}^{\mathrm{T}})\boldsymbol{\Sigma}_t(\alpha_{i,t}\boldsymbol{e})} + z_{i,t}^{\mathrm{g}} \tag{46}$$

$$r_{i,t} \ge \frac{1}{\sqrt{\varepsilon}}\sqrt{0^2 + (\alpha_{i,t}\boldsymbol{e}^{\mathrm{T}})\boldsymbol{\Sigma}_t(\alpha_{i,t}\boldsymbol{e})} + 0 \tag{47}$$

$$r_{i,t}^{\mathrm{RES}} = \alpha_{i,t}\sqrt{\frac{\boldsymbol{e}^{\mathrm{T}}\boldsymbol{\Sigma}_t\boldsymbol{e}}{\varepsilon}} \tag{48}$$

where $r_{i,t}^{\mathrm{RES}}$ is the reserve requirement.

According to the envelope theorem, the LMP $LMP_{i,t}$ can be obtained by taking the partial derivative of the Lagrangian function L with respect to the load, as shown in (49). The reserve price $LMP_{i,t}^{\mathrm{r}}$ can be obtained using (50).

$$LMP_{i,t} = \frac{\partial L}{\partial d_{i,t}} = \lambda_{i,t} \tag{49}$$

$$LMP_{i,t}^{\mathrm{r}} = \mu_{i,t}^{\mathrm{g,eq}} = \sqrt{\frac{\varepsilon}{\boldsymbol{e}\boldsymbol{\Sigma}_t\boldsymbol{e}^{\mathrm{T}}}}\left\{\lambda_t^{\alpha} - \sum_j 2\mu_{j,t}^{\mathrm{b}}[\boldsymbol{\Psi}_j(\boldsymbol{\alpha}\boldsymbol{e}^{\mathrm{T}} - \boldsymbol{I})]^{\mathrm{T}}\boldsymbol{\Psi}_j^{\mathrm{T}}\boldsymbol{\Sigma}\right\} \tag{50}$$

The LMUP describes the impact of uncertainty changes on the system cost. This price is related to the mean and standard deviation of the variables. In practice, the mean is often set to be zero, and the accuracy of load forecasts in

the electricity market typically does not fluctuate considerably. We mainly focus on studying the VPP uncertainty.

The LMUPs of VPP are defined as the partial derivative of the Lagrangian function given by (51) and (52). $UMP^{\mathrm{p}}_{k,t}$ is the LMUP considering the power uncertainty. The first component of $UMP^{\mathrm{p}}_{k,t}$ represents the price of the reserve cost allocated to the VPP uncertainty from the generator output. This price is paid to the generator by VPP. The second component of $UMP^{\mathrm{p}}_{k,t}$ represents the price of the reserve costs allocated to the VPP uncertainty from the grid lines. This is the price paid to grid by the VPP. $UMP^{\mathrm{e}}_{k,t}$ is the LMUP considering the energy uncertainty. Because of the VPP uncertainty, the range of energy constraints for the VPP may fluctuate, possibly increasing the overall system cost.

$$UMP^{\mathrm{p}}_{k,t}=\frac{\partial L}{\partial \sigma^{\mathrm{p}}_{k,t}}=\sum_{i}\frac{\mu^{\mathrm{g,eq}}_{i,t}\alpha_{i,t}\sigma^{\mathrm{p}}_{k,t}}{\sqrt{\varepsilon \boldsymbol{e}\boldsymbol{\Sigma}_t\boldsymbol{e}^{\mathrm{T}}}}+\sum_{j}2\mu^{\mathrm{b}}_{j,t}[\boldsymbol{\Psi}_j(\boldsymbol{I}-\boldsymbol{\alpha}\boldsymbol{e}^{\mathrm{T}})]^{\mathrm{T}}[\boldsymbol{\Psi}_j(\boldsymbol{I}-\boldsymbol{\alpha}\boldsymbol{e}^{\mathrm{T}})]\sigma^{\mathrm{p}}_{k,t} \tag{51}$$

$$UMP^{\mathrm{e}}_{k,t}=\frac{\partial L}{\partial \sigma^{\mathrm{e}}_{k,t}}=2\mu^{\mathrm{e}}_{j,t}\sigma^{\mathrm{e,t}}_{k,t}=2\mu^{\mathrm{e}}_{j,t}\sqrt{\sum_{\tau=1}^{T-t}\left(\prod_{\upsilon=1}^{\tau}\theta_{i,\upsilon}\right)^2\left(x^{b}_{i,\tau}\eta^{b}_{i}-\frac{x^{s}_{i,\tau}}{\eta^{s}_{i}}\right)^2(\sigma^{\mathrm{p}}_{k,t})^2+(\sigma^{\mathrm{e}}_{k,t})^2} \tag{52}$$

where $\sigma^{\mathrm{e,t}}_{k,t}$ is the standard deviation of the energy state of the k^{th} VPP at time t.

The total uncertainty payment for the VPPs and load is calculated using (53), which is allocated to entities providing reserve services, such as generators, energy storage systems, and other directly-connected power grids.

$$\begin{aligned}C_{\sigma}=&\Delta t\sum_{t}\sum_{k}(UMP^{\mathrm{p}}_{k,t}\cdot\sigma_{k,t}+UMP^{\mathrm{e}}_{k,t}\cdot\sigma^{\mathrm{e}}_{k,t})=\\&\Delta t\sum_{t}\sum_{i}\left(\alpha_{i,t}\lambda^{\alpha}_{t}-\sum_{j}2\alpha_{i,t}\mu^{\mathrm{b}}_{j,t}[\boldsymbol{\Psi}_j(\boldsymbol{\alpha}\boldsymbol{e}^{\mathrm{T}}-\boldsymbol{I})]^{\mathrm{T}}\boldsymbol{\Psi}^{\mathrm{T}}_{j}\boldsymbol{\Sigma}\right)+\\&\Delta t\sum_{t}\sum_{k}\sum_{j}2\mu^{\mathrm{b}}_{j,t}[\boldsymbol{\Psi}_j(\boldsymbol{I}-\boldsymbol{\alpha}\boldsymbol{e}^{\mathrm{T}})]^{\mathrm{T}}[\boldsymbol{\Psi}_j(\boldsymbol{I}-\boldsymbol{\alpha}\boldsymbol{e}^{\mathrm{T}})]\sigma^{2}_{k,t}+\\&\Delta t\sum_{t}\sum_{k}2\mu^{\mathrm{e}}_{k,\tau}(\sigma^{\mathrm{e,t}}_{k,t})^2\end{aligned} \tag{53}$$

where $\sigma_{k,t}$ is the standard deviation of the uncertainty source deviation.

Proposition 2 When no system congestion exists, the power uncertainty payment equals the reserve payment.

The proof is provided in Supplementary Material A, and it indicates that the LMUP is essentially the price generated by allocating reserve costs to each uncertainty source. The uncertainty payments are divided into three components: reserve, grid congestion, and energy uncertainty costs. Reserve costs are paid to the generators that provide reserves to the grid. Grid congestion and energy uncertainty costs are used to maintain grid stability and expand line capacity. Pricing uncertainty can provide price incentives for uncertainty sources, thereby promoting uncertainty reduction.

V. Case Study

In this section, we present a series of numerical results obtained for a 25-node power system to validate the effectiveness of the pricing strategy.

A. Environment and Settings of Test System

The simulations are conducted on a computer equipped with a 2.9 GHz Intel Core i9-12900H processor and 32 GB of RAM. The problem in the market clearing model is solved using the Gurobi V.10.0 optimizer. The market clearing model is executed in Python 3.10 on the Windows 11 operating system, utilizing the Gurobipy packages.

The one-line diagram of the 25-node power system is shown in Fig. 3. VPPs 1-6 (denoted as VPP#1-VPP#6) are connected to the grid at nodes 8, 10, 19, 15, 12, and 14, respectively. Generators 1-6 (denoted as GEN#1-GEN#6) are connected to the grid at nodes 23, 24, 25, 22, 21, and 20, respectively. The scheduling horizon T is set to be 24 hours. The market clearing is conducted hourly. The standard deviation of power uncertainty for each VPP is shown in Fig. 4. The load at each node is shown in Fig. 5. The ranges for the generator output power and VPP power are listed in Table II. The standard deviation of the load forecast for each node is set as $\sigma^{\mathrm{d}}_{i,t}=10\%\times d_{i,t}$. The standard deviation of the VPP energy boundaries is set as $\sigma^{\mathrm{e}}_{i,t}=3\%\times(\bar{e}_{i,t}-\underline{e}_{i,t})$.

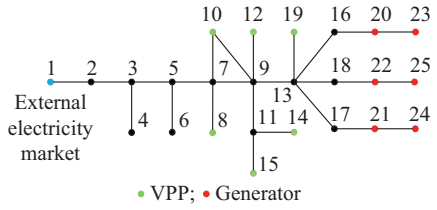

Fig. 3. One-line diagram of 25-node power system.

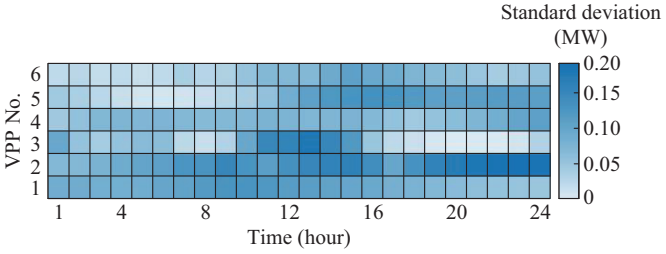

Fig. 4. Standard deviation of power uncertainty for each VPP.

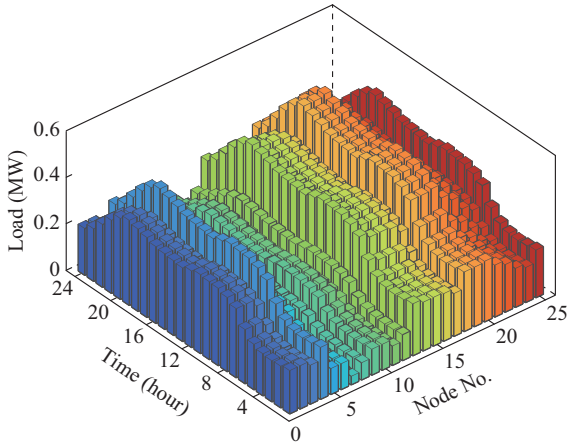

Fig. 5. Load at each node.

TABLE II
RANGE FOR GENERATOR OUTPUT POWER AND VPP POWER

Generator or VPP No.	Range (MW)	Generator or VPP No.	Range (MW)
GEN#1	0-2.0	VPP#1	−1.0-1.0
GEN#2	0-2.5	VPP#2	−1.0-1.0
GEN#3	0-2.5	VPP#3	−1.0-1.0
GEN#4	0-1.5	VPP#4	−0.5-0.5
GEN#5	0-2.0	VPP#5	−0.5-0.5
GEN#6	0-1.5	VPP#6	−0.5-0.5

The market clearing model is executed 100 times with different backgrounds. The time required to solve this model is shown in Fig. 6, where the average time is 11.79 s. The computation is efficient enough within the existing market framework.

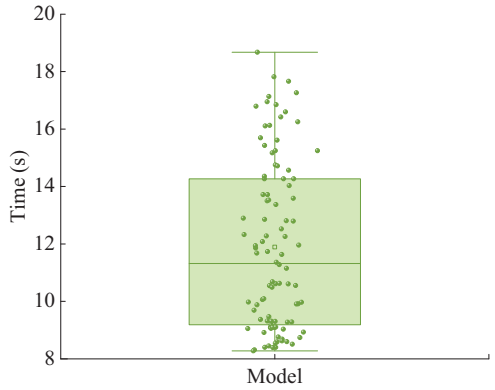

Fig. 6. Time required for solving market clearing model.

B. Market Clearing Results for EC-VPPs

Owing to system congestion, large differences occur between the market clearing and reserve prices across different nodes during certain periods. When the market clearing price is low, the purchasing behavior of the VPP can cause congestion at the generator nodes. Reserve prices increase because of congestion. Hence, even under congestion, the proposed pricing strategy can reflect the true value of distributed flexible resources. Figure 7 shows the LMPs in the electricity market, and Fig. 8 shows the reserve prices of the generators. After considering the correlation of node uncertainties, the reserve prices are shown in Supplementary Material B Figs. SB1 and SB2. The reserve prices under the joint chance constraints are shown in Supplementary Material B Figs. SB3 and SB4.

The total reserve payments of the VPP generally correspond to variations in power uncertainty. Compared with the reserve prices, the LMUP considering the power uncertainty of the VPP more accurately reflects the impact of its power uncertainty on the system. Table III lists the LMUP for VPP#2 and VPP#4 considering the power uncertainty. Although the overall uncertainty level of VPP#2 is higher than that of VPP#4, the LMUP of VPP#2 is consistently lower than that of VPP#4. This is because node 15 connected to VPP#4 experiences considerable congestion, which is also reflected in the market prices.

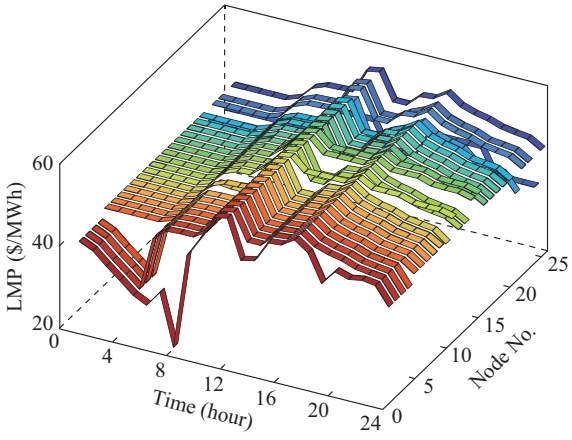

Fig. 7. LMPs in electricity market.

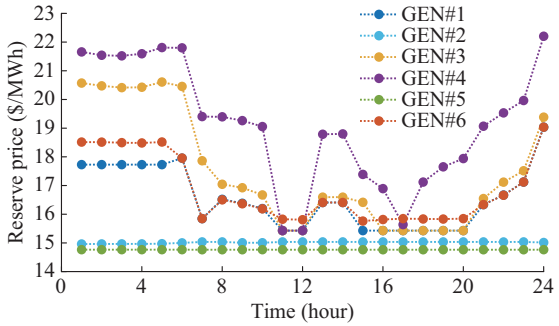

Fig. 8. Reserve prices of generators.

TABLE III
LMUP FOR VPP#2 AND VPP#4 CONSIDERING POWER UNCERTAINTY

Time (hour)	LMUP ($/MWh)		Time (hour)	LMUP ($/MWh)	
	VPP#2	VPP#4		VPP#2	VPP#4
1	19.22	18.00	13	17.10	26.48
2	19.73	18.95	14	17.16	25.45
3	20.14	19.75	15	17.48	17.81
4	20.42	19.57	16	15.60	16.02
5	20.58	19.23	17	15.57	15.45
6	21.29	19.23	18	15.67	16.38
7	20.45	16.11	19	15.73	19.18
8	26.85	16.71	20	15.72	21.56
9	27.58	16.50	21	17.71	24.17
10	16.58	23.63	22	17.74	26.84
11	15.55	15.48	23	19.35	29.86
12	15.56	15.46	24	24.84	36.66

Figure 9 shows the LMUPs of VPP calculated by (51). The LMUP considering the energy uncertainty for VPPs is zero during most periods because their energy levels are generally far from the constraint boundary, posing no risk of crossing. However, when the VPP energy level approaches the boundary, inherent uncertainty may introduce a risk of violation, affecting market clearing, and thus pricing should be applied during these periods. The system prices the VPP uncertainty when it affects market clearing, and it charges corresponding compensatory fees. This strategy transparently re-

flects the impact of each VPP uncertainty on the system across various time periods, encouraging VPPs to prioritize optimizing periods with greater potential revenue losses. Figure 10 shows the LMUPs of VPP calculated by (52).

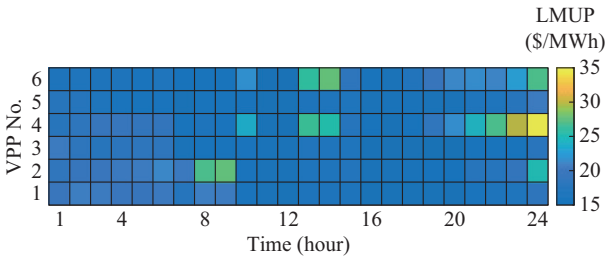

Fig. 9. LMUPs of VPP calculated by (51).

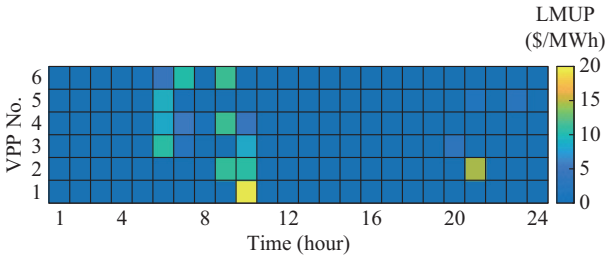

Fig. 10. LMUPs of VPP calculated by (52).

Table IV lists the payment amounts and percentages for components of uncertainty sources.

TABLE IV
PAYMENT AMOUNTS AND PERCENTAGES FOR COMPONENTS OF UNCERTAINTY SOURCES

Component	Amount ($)	Percentage (%)
Reserve cost	181.68	76
Congestion cost	31.45	13
Energy cost	26.99	11

A large portion of the total payments is allocated to reserve cost, indicating that the uncertainty generated in power has the greatest impact on market clearing. This amount is paid primarily to the generators that provide reserve services to the grid. In contrast, congestion costs appear across various time periods but are relatively low. This is because throughout market clearing, while network congestion occurs, it does not severely affect the operation of the grid or market clearing. On the other hand, energy costs exhibit the opposite characteristic, appearing relatively high only during specific periods. This is because the energy state of VPP rarely approaches its limits, making the impact of energy uncertainty on market clearing evident only during isolated periods. Figure 11 shows the payments for components of the uncertainty sources.

C. Results in Different Scenarios

The energy boundaries of VPPs vary with changes in their operating states, thereby increasing their flexibility and responsiveness to satisfy the dynamic demands of the electricity market.

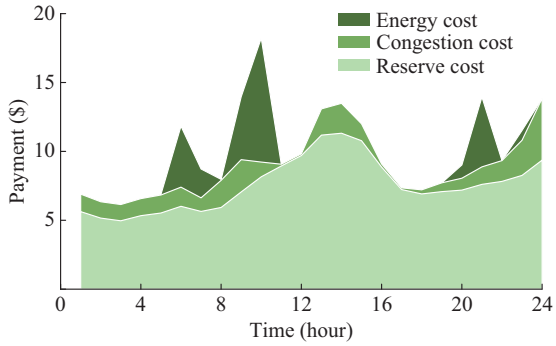

Fig. 11. Payment for components of uncertainty sources.

Figure 12 shows the energy state curves of VPP#4 with different risk tolerance levels ε. We assume that each set of uncertainty vectors of the VPP follows a normal distribution.

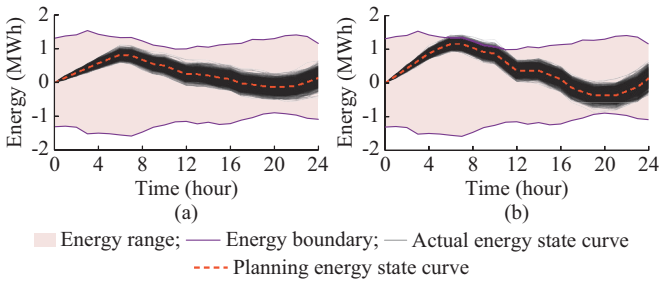

Fig. 12. Energy state curves of VPP#4 with different risk tolerance levels. (a) $\varepsilon = 0.05$. (b) $\varepsilon = 0.30$.

In Fig. 12(a), when $\varepsilon = 0.05$, the actual energy state curve of VPP#4 remains within the energy boundaries. VPP#4 has an energy overrun at Hour 10 when $\varepsilon = 0.30$ in Fig. 12(b). As the risk tolerance level increases, the likelihood of a VPP exceeding the energy boundaries also increases. In contrast, Table V shows that as the risk tolerance level decreases, the VPP revenue decreases, and the system cost increases.

TABLE V
SYSTEM SETTLEMENTS WITH DIFFERENT RISK TOLERANCE LEVELS

ε	System cost ($)	VPP revenue ($)
0.05	6824.92	165.86
0.30	6534.64	230.56

Uncertainty pricing has a positive effect on VPPs. In Fig. 13, the energy state of each VPP remains unchanged at the final time.

The uncertainty in VPP#1 varies depending on the standard deviation. As the uncertainty level increases, the planned revenue remains almost unchanged in the absence of payments for uncertainty. Considering the uncertain payments, large changes occur in the VPP#1 revenue. Both the total system and energy costs increase. This is because the increased uncertainty level affects the generator output, system congestion, and VPP energy constraints, leading to an increase in system costs.

Due to the uncertainty in the energy state constraint boundaries, the market charges compensatory fees to VPP.

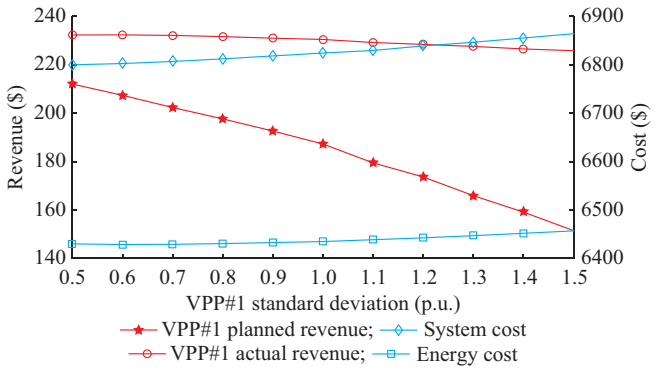

Fig. 13. Revenue and cost with different standard deviations (uncertainty levels).

We assume that the VPP energy boundary uncertainty follows a normal distribution, with $\sigma_{i,t}^{\mathrm{e}}=5\%\times(\bar{e}_{i,t}-\underline{e}_{i,t})$ and $\sigma_{k,t}^{\mathrm{p}}=0$. The upper and lower boundaries of the range are shifted by $n\sigma_{i,t}^{\mathrm{e}}$ toward the center. Table VI lists the system settlements under different energy boundary ranges. Note that $n\sigma_{i,t}^{\mathrm{e}}$ represents the degree of energy boundary reduction. As the energy boundary narrows, the VPP dispatching becomes more conservative, reducing the utilization rate of flexible resources. Finally, this leads to an increase in system costs and a reduction in VPP revenue.

TABLE VI
SYSTEM SETTLEMENTS UNDER DIFFERENT ENERGY BOUNDARY RANGES

n	System cost ($)	VPP revenue ($)
0	6617.84	375.08
3	6612.42	399.28
4	6615.32	395.42
5	6619.82	394.34

VI. CONCLUSION

We propose a DRCCO-based market clearing model for EC-VPPs and define the marginal price for uncertainties. The market clearing model includes uncertainties in VPP power and energy boundaries. Market operation results indicate that the proposed market clearing model provides fair incentives for both providers and uncertain sources. The proposed pricing strategy accurately reflects the true value of distributed flexible resources while guiding VPPs to minimize the forecasting errors and optimize the use of system transmission lines. Owing to uncertainties, both the overall system costs and VPP-related costs tend to increase. Owing to the pricing uncertainty, VPPs must cover the costs associated with their own uncertainties, which can reduce their revenues. The proposed pricing strategy incentivizes VPPs to properly manage their volatility, by either enhancing their forecasting techniques or investing in additional distributed flexible resources. This strategy safeguards the interests of both the electricity market and consumers, likely promoting more stable and efficient power systems.

The current chance-constrained method lacks detailed modeling of joint constraints. With the expansion of the electricity market and increasing participation of VPPs, solving the market clearing model under the mutual influence of chance constraints may become challenging. The solution to joint chance constraints has been a prominent research focus. In particular, the efficient solution of the joint chance constraints in VPPs remains unknown. Therefore, integrating the joint chance constraint approach is a promising topic for future research.

REFERENCES

[1] D. Zhao, V. Dvorkin, S. Delikaraoglou *et al*., "Uncertainty-informed renewable energy scheduling: a scalable bilevel framework," *IEEE Transactions on Energy Markets, Policy and Regulation*, vol. 2, no. 1, pp. 132-145, Mar. 2024.
[2] X. Yan, C. Gao, M. Song *et al*., "An IGDT-based day-ahead co-optimization of energy and reserve in a VPP considering multiple uncertainties," *IEEE Transactions on Industry Applications*, vol. 58, no. 3, pp. 4037-4049, May 2022.
[3] J. Liu, M. Li, F. Fang *et al*., "Review on virtual power plants," *Proceedings of the CSEE*, vol. 34, no. 29, pp. 5103-5111, Oct. 2014.
[4] J. Yu, Y. Liu, J. Yang *et al*., "Analysis of development of California ancillary service market and its enlightenment to China's power market," *Power System Technology*, vol. 43, no. 8, pp. 2711-2717, Jun. 2019.
[5] Y. He, Q. Chen, Y. Fei *et al*., "Typical foreign ancillary service market products and enlightenment to China," *Power System Technology*, vol. 42, no. 9, pp. 2915-2922, Jul. 2018.
[6] Y. He, M. Zhou, Z. Wu *et al*., "Study on operation mechanism of foreign representative balancing markets and its enlightenment for China," *Power System Technology*, vol. 42, no. 11, pp. 3520-3528, Nov. 2018.
[7] Z. Yi, Y. Xu, and W. Wu, "Market clearing strategy for distribution system considering multiple power commodities offered by virtual power plant," *Automation of Electric Power Systems*, vol. 44, no. 22, pp. 143-151, Jun. 2020.
[8] Z. Yi, Y. Xu, J. Zhou *et al*., "Bi-level programming for optimal operation of an active distribution network with multiple virtual power plants," *IEEE Transactions on Sustainable Energy*, vol. 11, no. 4, pp. 2855-2869, Oct. 2020.
[9] Z. Xu, H. Qu, W. Shao *et al*., "Virtual power plant-based pricing control for wind/thermal cooperated generation in China," *IEEE Transactions on Systems, Man, and Cybernetics: Systems*, vol. 46, no. 5, pp. 706-712, May 2016.
[10] D. S. Kirschen and G. Strbac, *Fundamentals of Power System Economics*. Hoboken: Wiley, 2018.
[11] Federal Energy Regulatory Commission. (2018, Feb.). Electric storage participation in markets operated by regional transmission organizations and independent system operators. [Online]. Available: https://www.ferc.gov/media/order-no-841
[12] Z. Yi, Y. Xu, W. Gu *et al*., "Aggregate operation model for numerous small-capacity distributed energy resources considering uncertainty," *IEEE Transactions on Smart Grid*, vol. 12, no. 5, pp. 4208-4224, Sept. 2021.
[13] Y. Wen, Z. Hu, and L. Liu, "Aggregate temporally coupled power flexibility of DERs considering distribution system security constraints," *IEEE Transactions on Power Systems*, vol. 38, no. 4, pp. 3884-3896, Jul. 2023.
[14] H. Zhao, B. Wang, X. Wang *et al*., "Active dynamic aggregation model for distributed integrated energy system as virtual power plant," *Journal of Modern Power Systems and Clean Energy*, vol. 8, no. 5, pp. 831-840, Sept. 2020.
[15] S. Wang and W. Wu, "Aggregate flexibility of virtual power plants with temporal coupling constraints," *IEEE Transactions on Smart Grid*, vol. 12, no. 6, pp. 5043-5051, Nov. 2021.
[16] F. Fang, S. Yu, and X. Xin, "Data-driven-based stochastic robust optimization for a virtual power plant with multiple uncertainties," *IEEE Transactions on Power Systems*, vol. 37, no. 1, pp. 456-466, Jan. 2022.
[17] Y. Zhang, F. Liu, Z. Wang *et al*., "Robust scheduling of virtual power plant under exogenous and endogenous uncertainties," *IEEE Transactions on Power Systems*, vol. 37, no. 2, pp. 1311-1325, Mar. 2022.
[18] R. Lu, T. Ding, B. Qin *et al*., "Multi-stage stochastic programming to joint economic dispatch for energy and reserve with uncertain renewable energy," *IEEE Transactions on Sustainable Energy*, vol. 11, no. 3, pp. 1140-1151, Jul. 2020.

[19] S. Jiang, J. Cheng, K. Pan *et al*., "Data-driven chance-constrained planning for distributed generation: a partial sampling approach," *IEEE Transactions on Power Systems*, vol. 38, no. 6, pp. 5228-5244, Nov. 2023.
[20] S. Wang, W. Wu, Q. Chen *et al*., "Stochastic flexibility evaluation for virtual power plants by aggregating distributed energy resources," *CSEE Journal of Power and Energy Systems*, vol. 10, no. 3, pp. 988-999, May 2024.
[21] C. Liu, C. Lee, H. Chen *et al*., "Stochastic robust mathematical programming model for power system optimization," *IEEE Transactions on Power Systems*, vol. 31, no. 1, pp. 821-822, Jan. 2016.
[22] N. G. Cobos, J. M. Arroyo, N. Alguacil *et al*., "Robust energy and reserve scheduling considering bulk energy storage units and wind uncertainty," *IEEE Transactions on Power Systems*, vol. 33, no. 5, pp. 5206-5216, Sept. 2018.
[23] W. Wei, F. Liu, and S. Mei, "Distributionally robust co-optimization of energy and reserve dispatch," *IEEE Transactions on Sustainable Energy*, vol. 7, no. 1, pp. 289-300, Jan. 2016.
[24] W. Xie and S. Ahmed, "Distributionally robust chance constrained optimal power flow with renewables: a conic reformulation," *IEEE Transactions on Power Systems*, vol. 33, no. 2, pp. 1860-1867, Mar. 2018.
[25] K. Long, Y. Yi, J. Cortés *et al*., "Safe and stable control synthesis for uncertain system models *via* distributionally robust optimization," in *Proceedings of 2023 American Control Conference*, San Diego, USA, May 2023, pp. 4651-4658.
[26] S. Ramyar, M. Tanaka, A. L. Liu *et al*., "Endogenous risk management of prosumers by distributionally robust chance-constrained optimization," *IEEE Transactions on Energy Markets*, *Policy and Regulation*, vol. 1, no. 1, pp. 48-59, Mar. 2023.
[27] X. Fang, B. M. Hodge, E. Du *et al*., "Introducing uncertainty components in locational marginal prices for pricing wind power and load uncertainties," *IEEE Transactions on Power Systems*, vol. 34, no. 3, pp. 2013-2024, May 2019.
[28] X. Fang, K. S. Sedzro, H. Yuan *et al*., "Deliverable flexible ramping products considering spatiotemporal correlation of wind generation and demand uncertainties," *IEEE Transactions on Power Systems*, vol. 35, no. 4, pp. 2561-2574, Jul. 2020.
[29] S. Majumder, S. A. Khaparde, A. P. Agalgaonkar *et al*., "Chance-constrained pre-contingency joint self-scheduling of energy and reserve in VPP," *IEEE Transactions on Power Systems*, vol. 39, no. 1, pp. 245-260, Jan. 2024.
[30] H. Wang, Z. Bie, and H. Ye, "Locational marginal pricing for flexibility and uncertainty with moment information," *IEEE Transactions on Power Systems*, vol. 38, no. 3, pp. 2761-2775, May 2023.
[31] W. Zhong, K. Xie, Y. Liu *et al*., "Chance constrained scheduling and pricing for multi-service battery energy storage," *IEEE Transactions on Smart Grid*, vol. 12, no. 6, pp. 5030-5042, Nov. 2021.
[32] X. Yan, C. Gao, M. Song *et al*., "An IGDT-based day-ahead co-optimization of energy and reserve in a VPP considering multiple uncertainties," *IEEE Transactions on Industry Applications*, vol. 58, no. 3, pp. 4037-4049, May 2022.
[33] M. Yazdaninejad, N. Amjady, and S. Dehghan, "VPP self-scheduling strategy using multi-horizon IGDT, enhanced normalized normal constraint, and bi-directional decision-making approach," *IEEE Transactions on Smart Grid*, vol. 11, no. 4, pp. 3632-3645, Jul. 2020.
[34] F. Fang, S. Yu, and X. Xin, "Data-driven-based stochastic robust optimization for a virtual power plant with multiple uncertainties," *IEEE Transactions on Power Systems*, vol. 37, no. 1, pp. 456-466, Jan. 2022.
[35] Z. Yi, Y. Xu, H. Wang *et al*., "Coordinated operation strategy for a virtual power plant with multiple DER aggregators," *IEEE Transactions on Sustainable Energy*, vol. 12, no. 4, pp. 2445-2458, Oct. 2021.
[36] H. Ye, Y. Ge, M. Shahidehpour *et al*., "Uncertainty marginal price, transmission reserve, and day-ahead market clearing with robust unit commitment," *IEEE Transactions on Power Systems*, vol. 32, no. 3, pp. 1782-1795, May 2017.
[37] Z. Yi, Y. Xu, W. Gu *et al*., "Aggregate operation model for numerous small-capacity distributed energy resources considering uncertainty," *IEEE Transactions on Smart Grid*, vol. 12, no. 5, pp. 4208-4224, Sept. 2021.
[38] W. Xie, S. Ahmed, and R. Jiang, "Optimized Bonferroni approximations of distributionally robust joint chance constraints," *Mathematical Programming*, vol. 191, no. 1, pp. 79-112, Jan. 2022.

Zhongkai Yi received the B.S. and M.S. degrees in electrical engineering from Harbin Institute of Technology, Harbin, China, in 2016 and 2018, respectively, and the Ph. D. degree in electrical engineering from Tsinghua University, Beijing, China, in 2022. He is currently an Associate Professor with the School of Electrical Engineering and Automation, Harbin Institute of Technology. His research interests include optimization and machine learning in power system.

Zihao Zhao received the B.S. degree in electrical engineering and automation from Harbin Institute of Technology, Harbin, China, in 2023. He is currently pursuing the master's degree in electrical engineering and automation from Harbin Institute of Technology. His research interests include control and optimization in power system and electricity market.

Ying Xu received the bachelor and Ph.D. degrees in electrical engineering and automation from Harbin Institute of Technology, Harbin, China, in 2003 and 2009, respectively. He is currently a Full Professor and Director with the Power System Research Institute in the School of Electrical Engineering and Automation, Harbin Institute of Technology. His research interests include power system control and optimization.

Yuhao Zhou received the B.S. and M.S. degrees in electrical engineering and automation from Harbin Institute of Technology, Harbin, China, in 2022 and 2024, respectively. He is currently working at State Grid Zhejiang Electric Power Co., Ltd., Ningbo, China. His research interests include optimization in power system and electricity market.

Lun Yang received the Ph.D. degree in electrical engineering from Tsinghua University, Beijing, China, in 2022. He is currently an Assistant Professor with the School of Automation Science and Engineering, Xi'an Jiaotong University, Xi'an, China. His research interests include optimization of power system and integrated energy system.